One-step Functionalization of Mildly and Strongly Reduced Graphene Oxide with Maleimide: An Experimental and Theoretical Investigation of the Diels-Alder [4+2] Cycloaddition Reaction

Alfonso Ferretti,[1] Sourab Sinha,[2] Luca Sagresti,[2,3] Esteban Araya-Hermosilla,[4] Mirko Prato,[5] Virgilio Mattoli,[4] Andrea Pucci,[5,6] and Giuseppe Brancato[2,3*]

1. *Università di Pisa, Dipartimento di Ingegneria Civile ed Industriale, Largo Lucio Lazzarino 2, I-56124 Pisa, Italy.*

2. *Scuola Normale Superiore, Piazza dei Cavalieri 7, I-56126 Pisa, Italy and CSGI.*

3. *Istituto Nazionale di Fisica Nucleare (INFN) sezione di Pisa, Largo Bruno Pontecorvo 3, 56127 Pisa, Italy.*

4. *Center for Materials Interfaces, Istituto Italiano di Tecnologia, Viale Rinaldo Piaggio 34, 56025 Pontedera, Italy.*

5. *Materials Characterization Facility, Istituto Italiano di Tecnologia, Via Morego 30, 16163 Genoa, Italy.*

6. *Department of Chemistry and Industrial Chemistry, University of Pisa, Via Moruzzi 13, 56124 Pisa, Italy.*

7. *CISUP, Centro per l'Integrazione della Strumentazione dell'Università di Pisa, Lungarno Pacinotti 43, 56126 Pisa, Italy.*

KEYWORDS

Reduced graphene oxide, Diels-Alder reaction, Maleimide, Defects, DFT, Kinetics

ABSTRACT

For large-scale graphene applications, such as the production of polymer-graphene nanocomposites, exfoliated graphene oxide (GO) and its reduced form (rGO) are presently considered very suitable starting material, showing enhanced chemical reactivity with respect to pristine graphene, in addition to peculiar electronic properties (i.e., tunable band gap). Among other chemical processes, a suitable way to obtain surface decoration of graphene is through direct one-step Diels-Alder (DA) reaction, e.g. through the use of dienophile or diene moieties. However, the feasibility and extent of decoration largely depends on the specific graphene microstructure that in the case of rGO sheets is not easy to control and generally presents a high degree of inhomogeneity owing to various on-plane functionalization (e.g., epoxide and hydroxyl groups) or in-plane lattice defects. In an effort to gain some insights on the covalent functionalization of variably reduced GO samples, we present a combined experimental and theoretical study on the DA cycloaddition reaction of maleimide, a dienophile functional unit well-suited for chemical conjugation of polymers and macromolecules. In particular, we considered both mildly and strongly reduced GOs. Using thermogravimetry, Raman and X-Ray photoelectron spectroscopy, and elemental analysis we show evidence of variable chemical reactivity of rGO as a function of the residual oxygen content. Moreover, from quantum mechanical calculations carried out at DFT level on different graphene reaction sites, we provide a more detailed molecular view to interpret experimental findings and to assess the reactivity series of different graphene modifications.

1. INTRODUCTION

In today graphene technology, a special role is played by chemically reduced exfoliated graphene oxide (rGO)[1]–[4] since this new class of materials enables low-cost and large-scale applications for a wide variety of use ranging from food packaging[5] to energy conservation[6] and from medical implants[7] to environmental protection.[8] Remarkably, in contrast to pristine graphene, rGO shows better dispersibility in water, polar organic solvents[9] and polymer matrices, which makes it more suitable for many applications as in nanocomposite materials,[1], [10] (bio)sensing,[11], [12] and drug delivery.[13] Besides, rGO shows an electronic band gap[14] that is befitting for carbon-based nanoelectronics.[15] Such enhanced properties depend ultimately on the presence of various oxygen-based groups (e.g, epoxide, hydroxyl, carboxyl, carbonyl, etc..) on the surface and/or edges of the graphene flakes, as a result of chemical oxidation of graphite followed by chemical and/or thermal reduction. These residual functional groups, which are non-homogeneously distributed[16] over the graphene surface leading to nonstoichiometric rGO sheets, do increase the effective interactions with other materials and, for example, favour the preparation of polymer-graphene nanocomposites through easy dispersion in polymeric matrices.

Another notable feature of the oxygen functional groups, as emerged in recent studies,[17]–[19] is the capability to greatly enhance the reactivity of graphene surface to "click" chemistry reactions, such as Diels-Alder (DA) [4+2] cycloadditions, thus opening up a new range of possibilities for graphene covalent functionalization under mild conditions and in absence of any catalyst. In pristine graphene, on the contrary, DA reactions occur more favourably only along flake edges or at local lattice defects rather than on surface interior regions, where non-covalent complexation is instead preferred.[20]–[22] This approach also contrasts other functionalization strategies that generally require more demanding reaction conditions and/or less straightforward protocols, as in case of highly reactive radicals such as hydrogenation[23], [24] or fluorination[25], [26] chemical addition reactions, such as 1,3-dipolar cycloaddition[27], [2+2] aryne cycloaddition[28], [2+1] nitrene cycloaddition, and so

on. In a DA reaction, graphene can act as either diene or dienophile and its dual nature was rationalized by the orbital symmetry and FMO theory.[29], [30] However, as noted above, non-functionalized and defect-free interior regions of graphene are quite inert to DA cycloadditions, since the corresponding reactions are highly endothermic under such conditions.[19] Local oxygen functionalization of the graphene surface, on the other hand, may turn DA cycloaddition reactions into an exothermic process, as found in recent studies of maleic anhydride cycloaddition,[18], [19] thus making covalent linking competitive towards non-covalent complexation.

Interestingly, previous studies[14], [31] demonstrated the effect of graphene oxygen functionalization on the fine modulation of the electronic band gap, an appealing property for nanoelectronics applications. In analogy to this, it would be interesting to assess whether the residual oxygen content can be used to tune the reactivity of the rGO surface and, therefore, to control the extent of decoration during covalent functionalization by e.g. polymers or supramolecular moieties exploiting "click" addition reactions.

In the present work, in an attempt to gain some further insights on graphene covalent functionalization, we carried out a combined experimental and theoretical study on the DA cycloaddition reaction of maleimide, a model dienophile moiety well-suited for covalently linking polymers or other complex macromolecules to graphene surface, to both mildly (i.e., prGO) and strongly (i.e., hrGO) reduced GO. Upon preparation of maleimide, we functionalized both rGO samples and characterized prGO-maleimide and hrGO-maleimide flakes using thermogravimetry (TGA), Raman and X-Ray photoelectron spectroscopy (XPS), and elemental analysis, thus obtaining evidence of a variable reactivity of rGO as a function of residual oxygen content. Furthermore, through density functional theory (DFT) calculations, we thoroughly investigated structure and energy stability of various maleimide-graphene adducts considering, for the sake of comparison, various types of modifications, such as pristine, defective and oxygen functionalized graphene models, and different surface and edge reaction sites. In a few cases leading to energetically favourable adducts, we also carried out

an analysis of the reaction barriers and corresponding kinetic rate constants. Overall, results helped to assess the reactivity series of different graphene modifications towards maleimide DA reaction and provided a molecular perspective to better interpret the experimental findings.

2. MATERIALS AND METHODS

2.1. Materials

Different reduced graphene oxide (rGO), i.e., partly reduced graphene oxide (prGO) and highly reduced graphene oxide (hrGO), were kindly provided by Abalonyx (Oslo, Norway). Briefly, rGO was prepared by introducing the dry graphene oxide powder into a quartz tube tubular oven (about 1 g/minute). The graphene oxide flashes in the hot zone and is then transported out of the tube by means of a continuous flow of air and collected on a filter. Residence time in the hot zone is estimated to be about 2 seconds. The oven temperature was set at 350 °C (air flux) and 1100 °C (argon flux), for prGO and hrGO, respectively. Toluene (99.5%), methanol (99.0%), 1-methyl-2-pyrrolidone (99.5%), and propylamine were used as received (Sigma-Aldrich, Italy). Maleic anhydride (Sigma-Aldrich, Italy) was purified by recrystallization before use.

2.2. Maleimide synthesis

Typically, 3.0 g of propylamine (0.050 mol) was dissolved in 250 mL of toluene, and then 6.0 g of maleic anhydride (0.061 mol) was added to the solution. The reaction mixture was stirred for 96 h. under reflux (130 °C). The solvent and the residual propylamine and maleic anhydride were removed under reduced pressure with a mechanical pump at 160 °C. The heating procedure allowed the conversion of the acid-amide open form into the cyclic imide. FTIR (cm^{-1}): 1780, 1710, 1385 and 1311. Anal. calcd for $C_7H_9NO_2$: C, 60.42; H, 6.52; N, 10.07; found: C, 60.30; H, 6.61; N, 9.97.

2.3. prGO and hrGO chemical functionalization

40 mg of maleimide and 10 mg of prGO or hrGO were dispersed in 20 mL of 1-methyl-2-pyrrolidone in a 30 mL centrifuge flask. The mixture was sonicated for 10 minutes at 400W

and 24 kHz with UP 400 S probe in titanium with a 3 mm diameter tip and 100 mm length (Hielscher's H3). During sonication, the flask was immersed in an ice bath to prevent excessive temperature rise (no adverse effects were found after sonication, Supporting Information Figure 1). Then, the dispersion was transferred in a 50 mL round bottom flask equipped with a stirring bar. The reaction was left to stir for 12 hours at 90 °C. After cooling, the rGO-maleimide were precipitated in 1L of deionized water and recovered by filtration using a sartorius filter (Durapore®) with a PVDF filter membrane with a pore size of 0.22 μm and a diameter of 47 mm. The products were dispersed in 250 mL of methanol to remove the unreacted maleimide, left under stirring overnight, and eventually recovered by filtration. The procedure of washing was repeated twice. The maleimide-rGOs products were then dried for 48 hours under vacuum and characterized by TGA, Raman spectroscopy, XPS and elemental analysis.

2.4. Maleimide-rGO characterization

ATR–FT–-IR spectra were recorded by means of a Perkin-Elmer Spectrum One (San Francisco, CA, USA), within the 4000–650 cm^{-1} and averaged over 32 scans. The elemental analysis was performed by using an Elementar Vario Micro Cube for oxygen, nitrogen, carbon and hydrogen. Thermal degradation of rGO was analyzed via thermogravimetric analysis (TGA) with a Mettler Toledo TGA/SDTA851 instrument (Mettler Toledo, Columbus, OH, USA) under nitrogen flux (60 mL/min). Raman spectroscopy has been performed using a Horiba Jobin Yvon Xplora ONE confocal Raman microscope (Horiba Scientific, Horiba Italy, Roma, Italy). The wavelength of the excitation laser was 542 nm and the power of the laser was kept below 1 mW to avoid sample heating.

Specimens for XPS analysis were prepared by pressing finely ground powders of the samples onto high purity indium pellets (>99.9% purity, Sigma). The XPS analysis were carried out with a Kratos Axis Ultra spectrometer using a monochromatic Al Kα source operated at 20 mA and 15 kV. Wide scan analyses were carried out with an analysis area of 300 x 700 microns and a pass energy of 160 eV. High resolution analyses were carried out with

2.5. Graphene molecular models

The process of oxidation, followed by chemical or thermal reduction, may introduce different type of modifications on graphene lattice and surface.[32] In addition, some lattice defects found in pristine graphene are likely present also in rGOs.[33] In order to assess the feasibility of maleimide DA cycloaddition reaction towards different graphene reaction sites, we considered a number of representative defect-free, defective and oxygen functionalized sites. To this end, a number of graphene molecular models were built up, as shown in Figure 1. In particular, we started from a 5×5 pristine graphene model (a nanoflake comprising 25 fused benzene rings), since a similar model was shown to provide reliable energetics in ref. [21]. Besides, we generated different models corresponding to single-vacancy defective sites (i.e., with a missing lattice carbon atom[34]–[36]), a double-vacancy site (i.e., formed either by coalescence of two single vacancies or by removing two neighbouring atoms), a Stone-Wales defect[37], a N-doped lattice[38] (i.e., with carbon replaced by nitrogen atom), and some oxygen functionalized sites, displaying covalently linked epoxide and/or hydroxyl groups. Dangling bonds of the single and double vacancies were saturated with hydrogen atoms.[39] Similarly, graphene edges (i.e., armchair and zigzag) were passivated with hydrogen atoms, since the main focus of the work was on the possibility of surface decoration.

2.6. Computational details

Quantum mechanical calculations were performed at DFT level, using the Minnesota hybrid functional (U)M06-2X[40], [41] in combination with the 6-311++G(d,p) basis set. The M062X functional was shown to predict well thermochemistry data[44] and a similar approach was already used to study graphene reactivity.[21], [42] The (open-shell) polyradical character of graphene, as found previously in graphene nanoflakes,[43] was taken into account by employing unrestricted DFT calculations. The broken-symmetry method was employed to properly study open-shell singlets. Optimized geometries of the ground and transition states of

the maleimide-adducts were computed and confirmed by normal mode analysis using a smaller basis set (i.e., 6-31G(d)). Note that in some test calculations we did not notice significant difference in geometries between the two basis sets, while energies were always reported with the larger one. Binding energies (ΔE) were computed using the super-molecular approach (i.e., for the reaction: $A + B \rightarrow AB$, $\Delta E_{AB} = E_{AB} - E_A - E_B$) with inclusion of zero-point energy. Moreover, the effect of the solvent on the adduct binding energy was evaluated using the conductor-like polarizable continuum model (CPCM)[44], by considering solvents of low (i.e., chloroform) and medium (i.e., acetonitrile) polarity. Reaction enthalpies and free energies for the maleimide DA cycloaddition reaction were estimated from binding energy calculations including thermal effects and, eventually, solvent contribution. In this case, we set the temperature to 50 °C (T = 323.15 K), since DA reactions are typically performed in a range of temperatures from 25 °C to 90 °C. Since test calculations showed that basically the same binding enthalpy is obtained when considering cycloaddition with both sides of maleimide, hereafter we reported only one binding mode. The open-shell singlet state was assumed as the most stable in all models in agreement with previous studies,[20], [21] with the exception of system 2R and 6R (i.e., doublet states) and system 10R (and corresponding transition states and products), whose triplet state was found as the most stable one (*vide infra*). Spin density isosurfaces were computed with the MultiWFN software.[45] All the calculations were performed using Gaussian16 software package.[46] Reaction rate constants were evaluated using the modified Arrhenius equation, also known as the Eyring-Polanyi equation, which follows the transition state theory (TST) to describe the variance of the rate of a reaction with temperature[47]:

$$k = \frac{k_B T}{h} e^{\frac{-\Delta G^{\#}}{RT}} \qquad (1)$$

where $\Delta G^{\#}$ is the Gibbs energy of activation, k_B is the Boltzmann's constant and h is the Planck's constant. Molecular models were represented graphically using the VMD software package.[48]

The reactivity of the local sites of the graphene sheet were analyzed using the condensed Fukui function (CFF),[49] which describes the electron density in a frontier orbital, as a result of a change in the total number of electrons. For a given atom, x, in a molecule with N_0 electrons in a constant external potential, $v(r)$, the CFF can be obtained from finite difference approximation (i.e., $\pm$ 1e) as:

$$f_x^+ = [\rho_x(N_0 + 1) - \rho_x(N_0)] \quad \text{(for nucleophilic attack)} \quad (2)$$

$$f_x^- = [\rho_x(N_0) - \rho_x(N_0 - 1)] \quad \text{(for electrophilic attack)} \quad (3)$$

where $\rho_x(N_0)$, $\rho_x(N_0 + 1)$ and $\rho_x(N_0 - 1)$ are the charge populations on atom x in the neutral, reduced and oxidized states of the molecule, respectively. From the CFFs, it is possible to obtain the local nucleophilicity and electrophilicity of the x atom by multiplying the global philicity as expressed by:

$$\omega = \left(\frac{\mu^2}{2\eta}\right)_{v(\vec{r})} \quad \text{(global philicity)} \quad (4)$$

$$\omega_x^{\pm} = f_x^{\pm}\omega \quad \text{(local nucleophilicity/electrophilicity)} \quad (5)$$

where η and μ are the global hardness and chemical potential, respectively, evaluated applying the finite difference method to the energies of the HOMO and LUMO according to the Koopman's theorem. The Hirshfeld charge population analysis (with hydrogen charges included in the heavy atoms) was used to evaluate the atomic charges.

3. RESULTS AND DISCUSSION

3.1. Maleimide synthesis

We prepared a maleimide derivative by modifying maleic anhydride with propylamine. We verified the success of the modification of maleic anhydride into maleimide via ATR-FT-IR (Supporting Information Figure 2). The most noticeable ATR-FT-IR results are the disappearance of the characteristics maleic anhydride peaks at 1860 and 1780 cm^{-1} and the appearance of the intense peak at 1710 cm^{-1}, the small peak at 1780 cm^{-1}, and medium peaks at around 1385 and 1311 cm^{-1} belonging to maleimide.[50] The elemental analysis eventually confirmed the purity of the prepared compound.

3.2. prGO and hrGO chemical functionalization

We used maleimide as a dienophile model to react with two types of rGO via the Diels-Alder cycloaddition reaction. prGO and hrGO were obtained from GO via a thermally reduced method at two different temperatures, i.e., 350 °C and 1100 °C, for prGO and hrGO, respectively. In particular, prGO shows a lower degree of reduction compared to hrGO. We confirmed it by elemental analysis and TGA. Figure 2 shows the TGA curves of the two different rGO and their respective residual mass. The weight loss is directly correlated to the amount of residual oxygen-containing groups. Thus, rGO with a more significant reduction extent should display a lower weight loss. Indeed, prGO had a residual mass of 72.08% in comparison with the 90.24% of hrGO. Moreover, prGO showed an inflection point at 218 °C that corresponds to the thermal decomposition of the oxygen-containing residual groups [51]. This is in agreement with the results provided by elemental analysis (Table 1), which shows hrGO composed by C and H, only, whereas oxygen residuals are present in prGO.

prGO and hrGO was then functionalized with maleimide to investigate the influence of defects on the rGO flakes in the Diels-Alder reaction. prGO-maleimide and hrGO-maleimide were characterized by TGA, Raman spectroscopy, XPS and elemental analysis. The structure of graphitic materials is commonly characterized by Raman spectroscopy. The most important peaks are the G and D bands in a rGO Raman spectrum [52][53], shown in Figure 3. The G-band centered around 1580 cm^{-1} represents the planar vibration of carbon atoms in most sp^2 graphitic materials. On the other hand, the disorder-induced D-band at 1340 cm^{-1} results from scattering defects that break the fundamental symmetry of the graphene sheet.[54],[55] Remarkably, the ratio of D and G band peak intensities (I_D/I_G) can be used as a standard index to detect defects on rGO. In this respect, the functionalization of prGO with maleimide inverts the intensities of the D and G-band, and the I_D/I_G ratio of prGO and maleimide-prGO changed from 0.94 to 0.87, respectively. This unexpected feature was already reported in the literature.[52] Aliphatic or aromatic functional groups in contact with the surface of the graphitic fillers effectively generate a more ordered structure, thus apparently limiting the

graphitic disorder of the graphene layer.[56] Surprisingly, hrGO shows a higher intensity of the D band and a G band shift to lower wavenumbers (blue shift) than prGO. We can associate the G band blue shift to the lower content of oxygen atoms in hrGO and the reestablishment of the graphite structure, and the D band intensity increase to the formation of new defects in the graphite structure during the reduction process.[57] The functionalization of hrGO with maleimide also inverted the intensities of D and G-bands, changing the I_D/I_G ratio of hrGO and hrGO-maleimide from 1.18 to 1.15, respectively. The low extent of the I_D/I_G ratio inversion in hrGO-maleimide compared to the prGO-maleimide product matches the latter's higher functionalization. We confirmed these results by performing elemental analysis (Table 1) that showed, in both cases, an overall increase of oxygen and nitrogen contents upon functionalization with maleimide. Nevertheless, such an increment was higher in the case of the prGO-maleimide adduct. This was again supported by TGA analysis, which revealed a larger degradation extent in this case.

To further investigate and quantify the type of defects on rGO samples before and after their functionalization with maleimide, a high-resolution XPS analysis was performed. Figure 4 shows the high-resolution data acquired over the binding energy regions typical for nitrogen and carbon main peaks, collected on the samples. The pristine prGO sample clearly shows signals that can be assigned to oxygen-containing functional groups, as summarized in Table 2. The amount of these groups strongly decreases in the hrGO sample. Indeed, the amount of C-O groups relative to the C=C network (i.e., [C-O]/[C=C]) is reduced from approx. 32% to 13%, similarly to the relative amount of C=O (i.e., [C=O]/[C=C]), which is reduced from approx. 11% to 5% and that of COOH (i.e., [COOH]/[C=C]) from 10% to 3%. It is worth noting that prGO contains a low amount of nitrogen (N 1s peak at 401.3 eV; [N]/[C=C] $\approx$ 0.8%), most likely in quaternary or graphitic state.[58] On the contrary, data collected on the hrGO sample do not show any nitrogen peak. The surface chemical composition of the prGO sample changed after the maleimide functionalization. The N 1s spectrum of the prGO-maleimide sample shows indeed an intense peak at (400.0±0.2) eV ([N]/[C=C] $\approx$ 7%),

corresponding to the pyrrolic-N of the imide ring[59] together with the quaternary N as seen in the prGO sample. At the same time, the relative concentration of the carbon component at 286 eV (assigned to C-O but also to C–N bonding of maleimide moieties[59] increased, thus confirming the successful functionalization. On the other hand, the chemical composition of the hrGO sample did not change significantly after functionalization. A low intensity N peak ([N]/[C=C] ≈ 0.5%) is, however, still visible at (400.1±0.2) eV, a result consistent with the presence of a low amount of maleimide. Therefore, XPS results confirmed a variable extent of functionalization of the rGO samples with maleimide, which is more effective for prGO as compared to hrGO.

3.3. Graphene molecular models

A total of 10 nanosized graphene models with various modifications were considered in the present work to investigate the DA cycloaddition by maleimide (Figure 1), as described in the Methods section. Since in some cases more than one binding site were evaluated (see description in Figure 1), overall 15 maleimide-graphene products were studied, including the non-covalent complexation for the sake of comparison. Note that the choice of the graphene binding sites was based, partially, on previously reported models[19] (oxygen-functionalized models) or suggested by a preliminary CFF analysis (*vide infra*), as in the case of the defective models. In all [4+2] Diels-Alder cycloaddition reactions, maleimide acted as a dienophile and graphene as a diene. The structure of the adducts are presented in Figure 4 and Supporting Information Figure 3-5. Both the external and internal (i.e., defective) edges of the graphene nanoflakes were saturated with hydrogens, which are omitted for clarity. Throughout the text, reactants and products are identified with a numbered label that follows the one assigned to the corresponding graphene model (note that R = reactant, TS = transition state, and P = product). In the following sections, we initially report and discuss the computed gas-phase reaction enthalpy at room temperature. Then, we consider the effect of solvent (i.e., chloroform and acetonitrile) and temperature on the DA cycloaddition reaction.

3.4. DA cycloaddition to defect-free sites

Investigation of maleimide DA cycloaddition to rGO sheet focused initially on defect-free sites (model 1R in Figure 1). Based on the known [4+2] DA reaction mechanism and previous studies, the dienophile moiety was expected to attack position 1,4 of the 6-member carbon rings. Single-layer graphene sheets are known to be planar, whereas the presence of defects (either missing carbon atoms or reconstructed non-hexagonal rings) may induce local curvature of the basal plane.[32], [33] However, at the local reaction sites, even pristine graphene model was observed to lose its planarity when covalently bound to maleimide. The local planarity (i.e., improper dihedral angle) of the sheet deviates from ~0° to ~30°, upon reaction with maleimide (Supporting Information Figure 3, 6 and Table 1). It was found that the dienophile moiety forms stable adducts only at specific sites, in agreement with previous studies on pristine graphene.[21] Indeed, a favourable interaction between defect-free sites and maleimide was observed only at the flake edge (marked in red in Figure 1), leading to corresponding adduct $1P_b$ (Supporting Information Figure 3c,d) with a binding energy of -12.2 kcal/mol (Figure 5). In particular, the latter adduct correspond to a DA cycloaddition at the zigzag step edge. On the other hand, other binding sites (i.e., $1P_a$ and $1P_c$) reported an unstable binding energy by more than 40 kcal/mol. This is also reflected on the estimated maleimide-graphene C-C bond distance, which was notably shorter in $1P_b$ (~1.58 Å) than for other adducts (1.63-1.65 Å) (Supporting Information Table 1). In all cases, the C=C bond in maleimide assumed a single bond character upon binding, going from 1.33 Å (isolated maleimide) to ~1.53 Å (bound maleimide). Note, also, that in all adducts the 1,4 carbon atoms of graphene hosting the dienophile moiety came closer to each other by about 0.20 Å (from ~2.8 Å to ~2.6 Å), an observation generally shared by all products under scrutiny in this work. Moreover, we noticed that in the formed adducts, maleimide molecular plane displayed an angle of roughly 26° with respect to the graphene sheet (Supporting Information Figure 3 and Table 1), an orientation that may have implications for maleimide conjugation with other molecular systems.

In case of non-covalent interactions, maleimide adopted a stacking configuration on top of the graphene sheet plane with a distance of 3.20 Å (Supporting Information Figure 4 and Table 1) and a binding energy of -9.6 kcal/mol (towards the edge, $1P_d$) and -16.0 kcal/mol (interior region, $1P_e$), in good agreement with results obtained by Cao *et. al*. [21] and Tang *et. al*. [19] for maleic anhydride.

3.5. DA cycloaddition to defective sites

Defective sites were found in pristine graphene and may also result from the oxidation and exfoliation process to generate GO sheets. Besides, some defective sites can be also generated upon reduction of oxygen-containing groups in the preparation of rGOs. In this work, we considered a few defective site models arising from single and double vacancy of the graphene lattice (i.e., 2R, 3R, 4R, and 5R) and one N-doped (6R) system. In 2R and 3R, the same local single-vacancy site was considered, though the former is a radical species while the latter is a closed-shell system as a result of addition of one hydrogen atom to the edge. Note that computed spin density isosurface of system 2R (Supporting Information Figure 7) revealed that the spin was mostly localized towards the nanoflake edge. The maleimide-graphene adducts resulted from reaction with defective system 2-4R reported negative reaction enthalpies (from -8.0 to -29.3 kcal/mol, Figure 5), in line with previous studies showing an increased reactivity of graphene defective sites with respect to (interior) defect-free sites.[42] Note that the choice of the binding site in the single-vacancy models (i.e., 2R and 3R) followed a different pattern (1-5 instead of 1-4 carbon-ring attack), since the usual 1-4 binding mode resulted in a unfavourable interaction with respect to the former (data not shown). It was reported that the formation energy of the double vacancy in graphene is thermodynamically favoured over the single vacancy by 4 eV.[60], [61] However, in the present study, it was observed that the ΔH of their adduct formation with maleimide did not differ much in case of the single vacancy radical system, 2P (ΔΔH(double vac. – single vac.) = -1.1 kcal/mol), while it was more significant for the closed-shell single vacancy system, 3P (ΔΔH(double vac. – single vac.) = +20.2 kcal/mol). The C-C bond distance between the diene and dienophile lie in

the range of 1.54-1.56 Å, but maleimide orientation in the adducts reported a somewhat larger tilting angle with respect to the cycloaddition products considered above (53-55°, Supporting Information Table 1). This is likely due to the unusual graphene local bending at the defective lattice sites. In contrast, the Stone-Wales defect (5R), which shows a reconstructed planar lattice, and the N-doped system (6R) both provided unfavourable binding energy (11.4 kcal/mol, 5P; 14.0 kcal/mol, 6P), as in defect-free pristine graphene (Figure 5). In all cases, a local out-of-plane displacement was observed in graphene lattice (~30°), accompanied by a slight shortening of the 1,4 carbon atom distance (~0.20 Å).

3.6. DA cycloaddition to oxygen functionalized sites

While various types of oxygen-based functional groups may occur as a result of oxidation and reduction of pristine graphene material, in this work we primarily focused on the most common surface modifications leading to the presence of epoxide and hydroxyl groups. Chemisorption of such functional groups onto graphene determines a change in carbon hybridization from sp^2 to sp^3 and, consequently, a local distortion of the 2D lattice structure. More importantly, the presence of epoxide and hydroxyl groups is expected to alter local site reactivity.[19] In this work, we considered a few representative models carrying either epoxide or hydroxyl groups, or both (system 7R-10R, Figure 1). When forming the corresponding maleimide-graphene adducts (Figure 4), we observed a significant sensitivity of the reaction enthalpy towards the specific functionalization and/or reaction site (Figure 5). The latter observation was apparent when comparing two binding sites on the same graphene model, namely 7aP and 7bP, which reported, respectively, a highly stable (7aP, -37.9 kcal/mol) and unstable (i.e., 7bP, 19.3 kcal/mol) product. In particular, favourable interactions were reported when maleimide was attached to carbon atoms both adjacent to oxygen-containing groups, as for systems 7aP, 8P, 9P, and 10P (Figure 5), leading to significantly negative reaction enthalpies ranging from -15 to -38 kcal/mol. Interestingly, stable maleimide-graphene products occurred in case of multiple functional groups clustered together, according to configurations

that seem not unlikely on the basis of the observed uneven distribution of oxygen-base groups.[16]

3.7. Thermal and solvent effects on reaction enthalpy

Furthermore, we evaluated the effect of solvent (i.e., chloroform and acetonitrile) and temperature on the computed reaction enthalpy (Figure 5 and Supporting Information Table 2). We found that, on average, inclusion of solvent effects (i.e., chloroform) led to reaction enthalpies less stable by about 1.3 kcal/mol, with a consistent destabilization in all models (from 0.1 to 5 kcal/mol) except for system 5R. On the other hand, thermal effects (from 0K to 323.15K) enhanced product stability by about 0.7 kcal/mol, with a similar effect in all systems considered. Hence, the introduction of both solvent and thermal effects, which partially compensate each other, provided an overall minor contribution to the computed reaction enthalpies (Figure 5). To proceed further, when we considered in a few test calculations a more polar solvent, such as acetonitrile, the effect resulted into a further decrease of the stability of the products, as seen in Supporting Information Table 2.

3.8. Thermochemical and kinetic analysis of the cycloaddition reaction

Considering only the DA cycloaddition reactions leading to favourable binding energies (i.e., exothermic reactions), we computed the corresponding transition states and energy barriers ($\Delta H^{\#}$). Results are summarized in Figure 6, where energy barriers are provided in both gas and solvent (i.e., chloroform) phases. Transition state models are depicted in Supporting Information Figure 8. Results can be grouped depending on the graphene model considered. In 1bP (edge binding), the cycloaddition reaction showed an activation barrier of 5.4 kcal/mol. In defective graphene models, the energy barrier spanned the range from 16.6 to 27.3 kcal/mol. On the other hand, in the case of the oxygen functionalized graphene systems, we found that the activation energy was significantly lower (i.e., 4.1 kcal/mol or less) in all models, with a barrierless reaction observed for model 7aP. Hence, the presence of epoxy and hydroxyl groups not only enhanced the stability of the maleimide-graphene adducts but made more feasible the covalent functionalization of rGO sheets with respect to the cycloaddition

reaction. These finding are in agreement with what reported by Tang *et. al.* [19] for DA cycloaddition reaction of maleic anhydride. Interestingly, the inclusion of solvent (i.e., chloroform) in transition state calculations washed out the energy barrier in one reaction with graphene oxide models (i.e., 8P), thus providing a significant boost to the DA cycloaddition kinetics. In contrast, solvent effects were of less importance for both defective and defect-free graphene models (Figure 6). Note that the role of solvent was often neglected and/or considered negligible in similar previous studies.[19], [21] Yet, our results may suggest that environmental effects could provide an appreciable contribution to the chemical reactivity of functionalized graphene sites typically occurring in rGOs. Besides, reaction and activation free energies were also evaluated and are reported in Supporting Information Table 3. Note that in this case the computed entropic contributions could be affected by larger errors than corresponding enthalpy estimates. Results show that entropic effects consistently destabilize products and transition states energies by about 15 kcal/mol. A significant destabilization was also found in the case of the non-covalent interaction, i.e. model 1Pe, for which binding free energy is reduced to -3.4 kcal/mol and -0.1 kcal/mol in gas-phase and chloroform, respectively. Hence, as noted above, covalent functionalization remained more favorable than non-covalent complexation. In addition, the rate constants of the DA cycloaddition reactions (Figure 6) were estimated on the basis of the corresponding Gibbs energy of activation and reported in Table 3.

Concerning the geometry of the transition state models, we found that the maleimide C=C bond was, as expected, intermediate between the isolated and the bound state with a distance of about 1.4 Å (Supporting Information Table 4). The C-C distance of the forming bonds between maleimide and graphene varied from about 1.6 Å to 2.6 Å, displaying either a symmetric (i.e., similar C-C distance) or a non-symmetric (i.e., one bond distance much shorter than the other one) configuration. Moreover, the local graphene out-of-plane angle (Supporting Information Table 4) was found to be closer to the planar geometry than the corresponding bound configuration (i.e., less than ~30°).

3.9 Graphene reactivity and binding energy

In an attempt to assess a correlation between the computed binding energy of the maleimide-graphene adducts and a suitable geometrical parameter, we considered the maleimide-graphene bond length in the adduct optimized structures (Supporting Information Table 1). In Supporting Information Figure 9, a plot displaying the binding enthalpy (Supporting Information Table 3) versus the maleimide-graphene bond length is depicted. In particular, we observed a good degree of correlation when considering only defect-free and defective graphene models (i.e., products with more negative binding enthalpies show smaller maleimide-graphene bond lengths). On the other hand, no correlation emerged from oxygen-functionalized graphene models.

Furthermore, we performed a CFF analysis (see Methods section for details) of the graphene nanoflakes in order to identify the more nucleophilic reactive sites on graphene, as this material acts as a diene in the DA cycloaddition with maleimide (i.e., the dienophile). Overall, the CFF analysis reported that the most prominent reactive sites are located at the graphene flake edges (i.e., where carbon atoms have a valence saturated with a hydrogen atom) and, in the interior region, in proximity of oxygen-containing functional groups, thus confirming the observed higher reactivity for the latter sites (Supporting Information Figures 10-14). In some cases, the CFF analysis seemed to predict well the more favorable binding sites for a given graphene model, as for model 1R (i.e., pristine graphene) where the carbon atoms with the more pronounced nucleophilic character are those involved in the DA cycloaddition to the external border (1Pb) (Supporting Information Figure 10a,b). In other cases, however, the CFF analysis did not highlight the significant difference observed in terms of maleimide-graphene energy stability, as in the case of model 7Pa versus model 7Pb (Supporting Information Figure 13a,b). Hence, our findings supported the use of the CFF analysis to obtain a qualitative indication of the preferred DA cycloaddition biding sites on graphene models.

4. CONCLUSIONS

In this work, we investigated the [4 + 2] Diels-Alder cycloaddition reaction of maleimide to both mildly (i.e., prGO) and strongly (i.e., hrGO) reduced GO by a combined experimental and theoretical study. Upon preparation of prGO-maleimide and hrGO-maleimide flakes, experimental characterization carried out by TGA, Raman spectroscopy, XPS and elemental analysis provided strong evidence of an increased reactivity of rGO as a function of residual oxygen content. Then, a detailed computational analysis of the maleimide DA cycloaddition towards various reaction site models, including pristine, defective and oxygen functionalized graphene, was carried out. Results revealed that exothermic reactions significantly more favourable than non-covalent complexation (ΔH = -16 kcal/mol) are those with graphene lattice vacancies or equipped with local oxygen groups ($\Delta H \sim$ -30-40 kcal/mol), in agreement with recent studies on DA cycloadditions to graphene. Yet, our *in silico* investigation highlighted that, in terms of activation energy, graphene sites functionalized with oxygen (i.e., epoxy and/or hydroxyl groups) are definitely the more reactive ones showing either small (3-4 kcal/mol) or no reaction barriers upon maleimide DA cycloaddition. This may be an important point to consider when processing graphene for nanocomposite preparation. Besides, the role of thermal and solvent effects was also carefully examined in our work. Temperature and environment do not change dramatically the product stability with respect to reagents, but in one case inclusion of chloroform was observed to boost DA cycloaddition by lowering the corresponding activation barrier. This may suggest that solvent effects could not be safely ignored, as typically done in computational studies, though further investigation are required to fully clarify possible environmental effects on the DA cycloaddition reaction.

Overall, our results corroborated previous evidence of an enhanced reactivity of graphene oxides[17]–[19] and, at the same time, provided further insights on the relation between extent of functionalization and residual oxygen content. Therefore, in addition to other preparation strategies, our work suggests that the extent of rGO functionalization might be controlled by fine tuning the chemical and/or thermal reduction of the starting graphene oxide

material. Besides, by varying the residual oxygen content of rGO, the electronic properties of the resulting nanomaterial can be also effectively tuned, therefore both effects (enhanced reactivity and tunable band gap) could be exploited in carbon-based nanoelectronics applications.

5. ACKNOWLEDGEMENTS

6. REFERENCES

[1] S. Stankovich *et al.*, "Graphene-based composite materials," *Nature*, vol. 442, no. 7100, pp. 282–286, Jul. 2006, doi: 10.1038/nature04969.

[2] G. Eda, G. Fanchini, and M. Chhowalla, "Large-area ultrathin films of reduced graphene oxide as a transparent and flexible electronic material," *Nature Nanotech*, vol. 3, no. 5, pp. 270–274, May 2008, doi: 10.1038/nnano.2008.83.

[3] P. Ranjan, S. Agrawal, A. Sinha, T. R. Rao, J. Balakrishnan, and A. D. Thakur, "A Low-Cost Non-explosive Synthesis of Graphene Oxide for Scalable Applications," *Sci Rep*, vol. 8, no. 1, p. 12007, Aug. 2018, doi: 10.1038/s41598-018-30613-4.

[4] R. Tarcan, O. Todor-Boer, I. Petrovai, C. Leordean, S. Astilean, and I. Botiz, "Reduced graphene oxide today," *J. Mater. Chem. C*, vol. 8, no. 4, pp. 1198–1224, Jan. 2020, doi: 10.1039/C9TC04916A.

[5] A. Barra *et al.*, "Graphene Derivatives in Biopolymer-Based Composites for Food Packaging Applications," *Nanomaterials*, vol. 10, no. 10, Art. no. 10, Oct. 2020, doi: 10.3390/nano10102077.

[6] L. Wang *et al.*, "Graphene oxide as an ideal substrate for hydrogen storage," *ACS Nano*, vol. 3, no. 10, pp. 2995–3000, Oct. 2009, doi: 10.1021/nn900667s.

[7] M. Li *et al.*, "An overview of graphene-based hydroxyapatite composites for orthopedic applications," *Bioactive Materials*, vol. 3, no. 1, pp. 1–18, Mar. 2018, doi: 10.1016/j.bioactmat.2018.01.001.

[8] F. Li, X. Jiang, J. Zhao, and S. Zhang, "Graphene oxide: A promising nanomaterial for energy and environmental applications," *Nano Energy*, vol. C, no. 16, pp. 488–515, 2015, doi: 10.1016/j.nanoen.2015.07.014.

[9] J. I. Paredes, S. Villar-Rodil, A. Martínez-Alonso, and J. M. D. Tascón, "Graphene Oxide Dispersions in Organic Solvents," *Langmuir*, vol. 24, no. 19, pp. 10560–10564, Oct. 2008, doi: 10.1021/la801744a.

[10] E. A. Araya-Hermosilla, M. Carlotti, F. Picchioni, V. Mattoli, and A. Pucci, "Electrically-Conductive Polyketone Nanocomposites Based on Reduced Graphene Oxide," *Polymers*, vol. 12, no. 4, Art. no. 4, Apr. 2020, doi: 10.3390/polym12040923.

[11] C.-H. Lu, H.-H. Yang, C.-L. Zhu, X. Chen, and G.-N. Chen, "A graphene platform for sensing biomolecules," *Angew Chem Int Ed Engl*, vol. 48, no. 26, pp. 4785–4787, 2009, doi: 10.1002/anie.200901479.

[12] E. Araya-Hermosilla, M. Minichino, V. Mattoli, and A. Pucci, "Chemical and Temperature Sensors Based on Functionalized Reduced Graphene Oxide," *Chemosensors*, vol. 8, no. 2, Art. no. 2, Jun. 2020, doi: 10.3390/chemosensors8020043.

[13] Z. Liu, J. T. Robinson, X. Sun, and H. Dai, "PEGylated Nanographene Oxide for Delivery of Water-Insoluble Cancer Drugs," *J. Am. Chem. Soc.*, vol. 130, no. 33, pp. 10876–10877, Aug. 2008, doi: 10.1021/ja803688x.

[14] H. Huang, Z. Li, J. She, and W. Wang, "Oxygen density dependent band gap of reduced graphene oxide," *Journal of Applied Physics*, vol. 111, no. 5, p. 054317, Mar. 2012, doi: 10.1063/1.3694665.

[15] D.-J. Kim, I. Y. Sohn, J.-H. Jung, O. J. Yoon, N.-E. Lee, and J.-S. Park, "Reduced graphene oxide field-effect transistor for label-free femtomolar protein detection," *Biosensors and Bioelectronics*, vol. 41, pp. 621–626, Mar. 2013, doi: 10.1016/j.bios.2012.09.040.

[16] D. S. Shin *et al.*, "Distribution of oxygen functional groups of graphene oxide obtained from low-temperature atomic layer deposition of titanium oxide," *RSC Adv.*, vol. 7, no. 23, pp. 13979–13984, Feb. 2017, doi: 10.1039/C7RA00114B.

[17] J. Yuan, G. Chen, W. Weng, and Y. Xu, "One-step functionalization of graphene with cyclopentadienyl-capped macromolecules via Diels–Alder 'click' chemistry," *J. Mater. Chem.*, vol. 22, no. 16, pp. 7929–7936, Mar. 2012, doi: 10.1039/C2JM16433G.

[18] P. P. Brisebois, C. Kuss, S. B. Schougaard, R. Izquierdo, and M. Siaj, "New Insights into the Diels–Alder Reaction of Graphene Oxide," *Chemistry – A European Journal*, vol. 22, no. 17, pp. 5849–5852, 2016, doi: 10.1002/chem.201504984.

[19] S. Tang, W. Wu, L. Liu, Z. Cao, X. Wei, and Z. Chen, "Diels–Alder reactions of graphene oxides: greatly enhanced chemical reactivity by oxygen-containing groups," *Phys. Chem. Chem. Phys.*, vol. 19, no. 18, pp. 11142–11151, 2017, doi: 10.1039/C7CP01086A.

[20] S. Bian *et al.*, "Covalently Patterned Graphene Surfaces by a Force-Accelerated Diels–Alder Reaction," *J. Am. Chem. Soc.*, vol. 135, no. 25, pp. 9240–9243, Jun. 2013, doi: 10.1021/ja4042077.

[21] Y. Cao, S. Osuna, Y. Liang, R. C. Haddon, and K. N. Houk, "Diels–Alder Reactions of Graphene: Computational Predictions of Products and Sites of Reaction," *J. Am. Chem. Soc.*, vol. 135, no. 46, pp. 17643–17649, Nov. 2013, doi: 10.1021/ja410225u.

[22] P. A. Denis, "Organic Chemistry of Graphene: The Diels-Alder Reaction," *Chemistry – A European Journal*, vol. 19, no. 46, pp. 15719–15725, 2013, doi: 10.1002/chem.201302622.

[23] J. T. Robinson *et al.*, "Properties of Fluorinated Graphene Films," *Nano Lett.*, vol. 10, no. 8, pp. 3001–3005, Aug. 2010, doi: 10.1021/nl101437p.

[24] S. B. Bon *et al.*, "Plasma Fluorination of Chemically Derived Graphene Sheets and Subsequent Modification With Butylamine," *Chem. Mater.*, vol. 21, no. 14, pp. 3433–3438, Jul. 2009, doi: 10.1021/cm901039j.

[25] R. Balog *et al.*, "Bandgap opening in graphene induced by patterned hydrogen adsorption," *Nature Mater*, vol. 9, no. 4, pp. 315–319, Apr. 2010, doi: 10.1038/nmat2710.

[26] Z. Yang, Y. Sun, L. B. Alemany, T. N. Narayanan, and W. E. Billups, "Birch Reduction of Graphite. Edge and Interior Functionalization by Hydrogen," *J. Am. Chem. Soc.*, vol. 134, no. 45, pp. 18689–18694, Nov. 2012, doi: 10.1021/ja3073116.

[27] V. Georgakilas *et al.*, "Organic functionalisation of graphenes," *Chem. Commun.*, vol. 46, no. 10, p. 1766, 2010, doi: 10.1039/b922081j.

[28] X. Zhong *et al.*, "Aryne cycloaddition: highly efficient chemical modification of graphene," *Chem. Commun.*, vol. 46, no. 39, p. 7340, 2010, doi: 10.1039/c0cc02389b.

[29] S. Sarkar, E. Bekyarova, S. Niyogi, and R. C. Haddon, "Diels−Alder Chemistry of Graphite and Graphene: Graphene as Diene and Dienophile," *J. Am. Chem. Soc.*, vol. 133, no. 10, pp. 3324–3327, Mar. 2011, doi: 10.1021/ja200118b.

[30] S. Sarkar, E. Bekyarova, and R. C. Haddon, "Chemistry at the Dirac Point: Diels–Alder Reactivity of Graphene," *Acc. Chem. Res.*, vol. 45, no. 4, pp. 673–682, Apr. 2012, doi: 10.1021/ar200302g.

[31] T. Takahashi, K. Sugawara, E. Noguchi, T. Sato, and T. Takahashi, "Band-gap tuning of monolayer graphene by oxygen adsorption," *Carbon*, vol. 73, pp. 141–145, Jul. 2014, doi: 10.1016/j.carbon.2014.02.049.

[32] P. Feicht and S. Eigler, "Defects in Graphene Oxide as Structural Motifs," *ChemNanoMat*, vol. 4, no. 3, pp. 244–252, 2018, doi: 10.1002/cnma.201700357.

[33] F. Banhart, J. Kotakoski, and A. V. Krasheninnikov, "Structural Defects in Graphene," *ACS Nano*, vol. 5, no. 1, pp. 26–41, Jan. 2011, doi: 10.1021/nn102598m.

[34] J. C. Meyer, C. Kisielowski, R. Erni, M. D. Rossell, M. F. Crommie, and A. Zettl, "Direct Imaging of Lattice Atoms and Topological Defects in Graphene Membranes," *Nano Lett.*, vol. 8, no. 11, pp. 3582–3586, Nov. 2008, doi: 10.1021/nl801386m.

[35] M. H. Gass, U. Bangert, A. L. Bleloch, P. Wang, R. R. Nair, and A. K. Geim, "Free-standing graphene at atomic resolution," *Nature Nanotech*, vol. 3, no. 11, pp. 676–681, Nov. 2008, doi: 10.1038/nnano.2008.280.

[36] M. M. Ugeda, I. Brihuega, F. Guinea, and J. M. Gómez-Rodríguez, "Missing Atom as a Source of Carbon Magnetism," *Phys. Rev. Lett.*, vol. 104, no. 9, p. 096804, Mar. 2010, doi: 10.1103/PhysRevLett.104.096804.

[37] A. J. Stone and D. J. Wales, "Theoretical studies of icosahedral C60 and some related species," *Chemical Physics Letters*, vol. 128, no. 5–6, pp. 501–503, Aug. 1986, doi: 10.1016/0009-2614(86)80661-3.

[38] D. Wei, Y. Liu, Y. Wang, H. Zhang, L. Huang, and G. Yu, "Synthesis of N-Doped Graphene by Chemical Vapor Deposition and Its Electrical Properties," *Nano Lett.*, vol. 9, no. 5, pp. 1752–1758, May 2009, doi: 10.1021/nl803279t.

[39] P. Koskinen, S. Malola, and H. Häkkinen, "Self-Passivating Edge Reconstructions of Graphene," *Phys. Rev. Lett.*, vol. 101, no. 11, p. 115502, Sep. 2008, doi: 10.1103/PhysRevLett.101.115502.

[40] Y. Zhao and D. G. Truhlar, "The M06 suite of density functionals for main group thermochemistry, thermochemical kinetics, noncovalent interactions, excited states, and transition elements: two new functionals and systematic testing of four M06-class functionals and 12 other functionals," *Theor Chem Account*, vol. 120, no. 1–3, pp. 215–241, May 2008, doi: 10.1007/s00214-007-0310-x.

[41] N. Mardirossian and M. Head-Gordon, "Thirty years of density functional theory in computational chemistry: an overview and extensive assessment of 200 density functionals," *Molecular Physics*, vol. 115, no. 19, pp. 2315–2372, Oct. 2017, doi: 10.1080/00268976.2017.1333644.

[42] P. A. Denis and F. Iribarne, "Comparative Study of Defect Reactivity in Graphene," *J. Phys. Chem. C*, vol. 117, no. 37, pp. 19048–19055, Sep. 2013, doi: 10.1021/jp4061945.

[43] F. Plasser *et al.*, "The Multiradical Character of One- and Two-Dimensional Graphene Nanoribbons," *Angew. Chem. Int. Ed.*, vol. 52, no. 9, pp. 2581–2584, Feb. 2013, doi: 10.1002/anie.201207671.

[44] V. Barone and M. Cossi, "Quantum Calculation of Molecular Energies and Energy Gradients in Solution by a Conductor Solvent Model," *J. Phys. Chem. A*, vol. 102, no. 11, pp. 1995–2001, Mar. 1998, doi: 10.1021/jp9716997.

[45] T. Lu and F. Chen, "Multiwfn: A multifunctional wavefunction analyzer," *Journal of Computational Chemistry*, vol. 33, no. 5, pp. 580–592, 2012, doi: 10.1002/jcc.22885.

[46] M. Frisch *et al.*, "Gaussian 16 Revision C. 01. 2016; Gaussian Inc," *Wallingford CT*, vol. 29.

[47] H. Eyring, "The Activated Complex in Chemical Reactions," *The Journal of Chemical Physics*, vol. 3, no. 2, pp. 107–115, Feb. 1935, doi: 10.1063/1.1749604.

[48] W. Humphrey, A. Dalke, and K. Schulten, "VMD: visual molecular dynamics," *J Mol Graph*, vol. 14, no. 1, pp. 33–38, 27–28, Feb. 1996.

[49] Weitao. Yang and W. J. Mortier, "The use of global and local molecular parameters for the analysis of the gas-phase basicity of amines," *J. Am. Chem. Soc.*, vol. 108, no. 19, pp. 5708–5711, Sep. 1986, doi: 10.1021/ja00279a008.

[50] L. M. Polgar, M. van Duin, A. A. Broekhuis, and F. Picchioni, "Use of Diels–Alder Chemistry for Thermoreversible Cross-Linking of Rubbers: The Next Step toward Recycling of Rubber Products?," *Macromolecules*, vol. 48, no. 19, pp. 7096–7105, Oct. 2015, doi: 10.1021/acs.macromol.5b01422.

[51] B. D. Ossonon and D. Bélanger, "Synthesis and characterization of sulfophenyl-functionalized reduced graphene oxide sheets," *RSC Advances*, vol. 7, no. 44, 2017, doi: 10.1039/c6ra28311j.

[52] J. Bin Wu, M. L. Lin, X. Cong, H. N. Liu, and P. H. Tan, "Raman spectroscopy of graphene-based materials and its applications in related devices," *Chemical Society Reviews*, vol. 47, no. 5. 2018. doi: 10.1039/c6cs00915h.

[53] O. Vryonis, T. Andritsch, A. S. Vaughan, and P. L. Lewin, "An alternative synthesis route to graphene oxide: influence of surface chemistry on charge transport in epoxy-based composites," *Journal of Materials Science*, vol. 54, no. 11, 2019, doi: 10.1007/s10853-019-03477-w.

[54] S. Muhammad Hafiz *et al.*, "A practical carbon dioxide gas sensor using room-temperature hydrogen plasma reduced graphene oxide," *Sensors and Actuators, B: Chemical*, vol. 193, 2014, doi: 10.1016/j.snb.2013.12.017.

[55] L. G. Cançado *et al.*, "Quantifying defects in graphene via Raman spectroscopy at different excitation energies," *Nano Letters*, vol. 11, no. 8, 2011, doi: 10.1021/nl201432g.

[56] X. Qi *et al.*, "Conjugated-polyelectrolyte-functionalized reduced graphene oxide with excellent solubility and stability in polar solvents," *Small*, vol. 6, no. 5, 2010, doi: 10.1002/smll.200902221.

[57] R. Muzyka, S. Drewniak, T. Pustelny, M. Chrubasik, and G. Gryglewicz, "Characterization of graphite oxide and reduced graphene oxide obtained from different graphite precursors and oxidized by different methods using Raman spectroscopy," *Materials*, vol. 11, no. 7, 2018, doi: 10.3390/ma11071050.

[58] T. Pillar-Little and D. Y. Kim, "Differentiating the impact of nitrogen chemical states on optical properties of nitrogen-doped graphene quantum dots," *RSC Adv.*, vol. 7, no. 76, pp. 48263–48267, Oct. 2017, doi: 10.1039/C7RA09252K.

[59] J.-M. Seo and J.-B. Baek, "A solvent-free Diels–Alder reaction of graphite into functionalized graphene nanosheets," *Chemical Communications*, vol. 50, no. 93, pp. 14651–14653, 2014, doi: 10.1039/C4CC07173E.

[60] A. A. El-Barbary, R. H. Telling, C. P. Ewels, M. I. Heggie, and P. R. Briddon, "Structure and energetics of the vacancy in graphite," *Phys. Rev. B*, vol. 68, no. 14, p. 144107, Oct. 2003, doi: 10.1103/PhysRevB.68.144107.

[61] A. V. Krasheninnikov, P. O. Lehtinen, A. S. Foster, and R. M. Nieminen, "Bending the rules: Contrasting vacancy energetics and migration in graphite and carbon nanotubes," *Chemical Physics Letters*, vol. 418, no. 1–3, pp. 132–136, Jan. 2006, doi: 10.1016/j.cplett.2005.10.106.
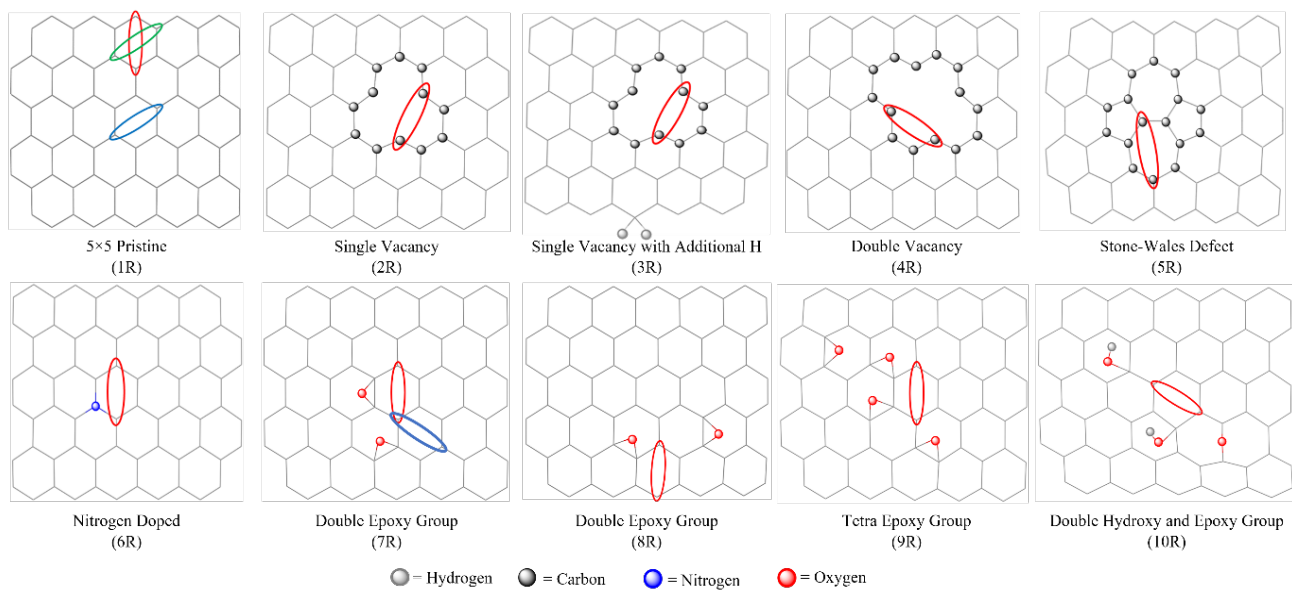
Figure 1 Defective, functionalized and defect-free graphene reaction sites considered in this study. The depicted coloured circles identify the pair of carbon atoms on each graphene model which are considered in the DA reaction with maleimide.
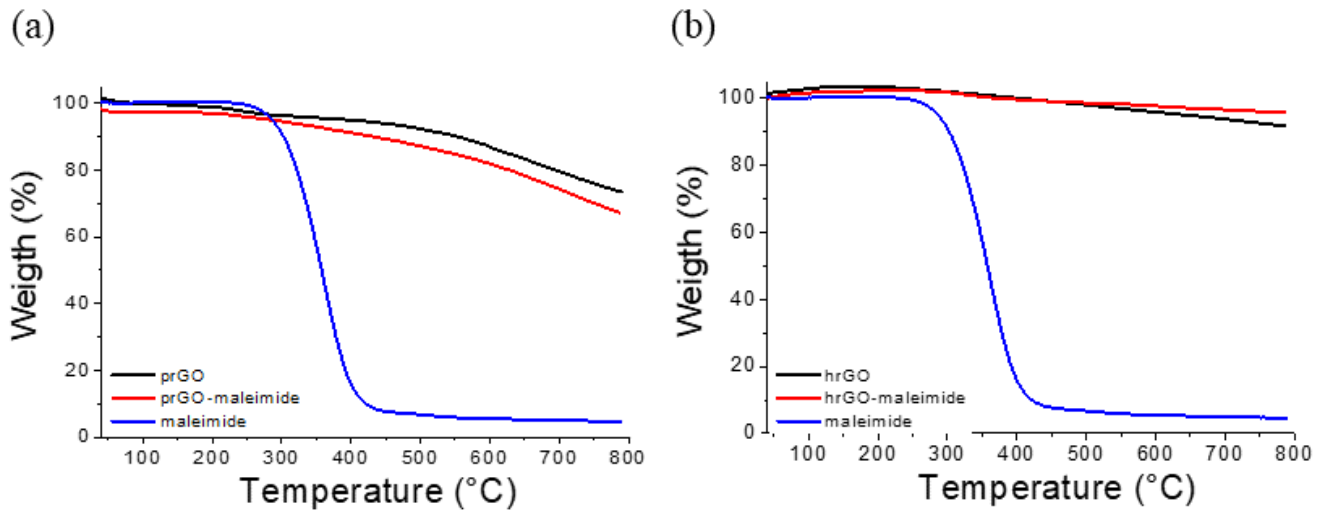
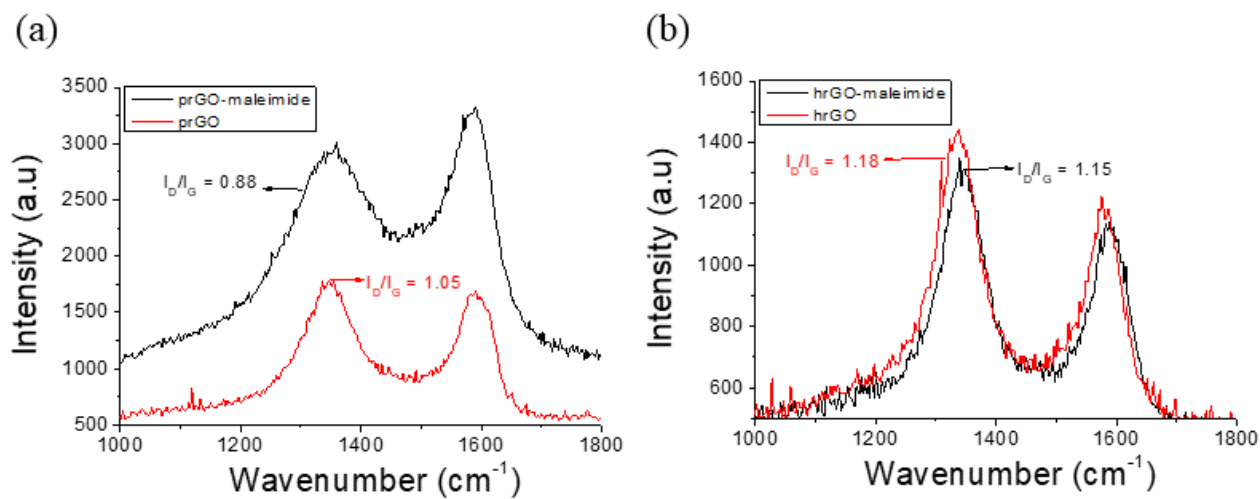**Figure 2** Thermogravimetric analysis of (a) prGO and (b) hrGO functionalized with maleimide.

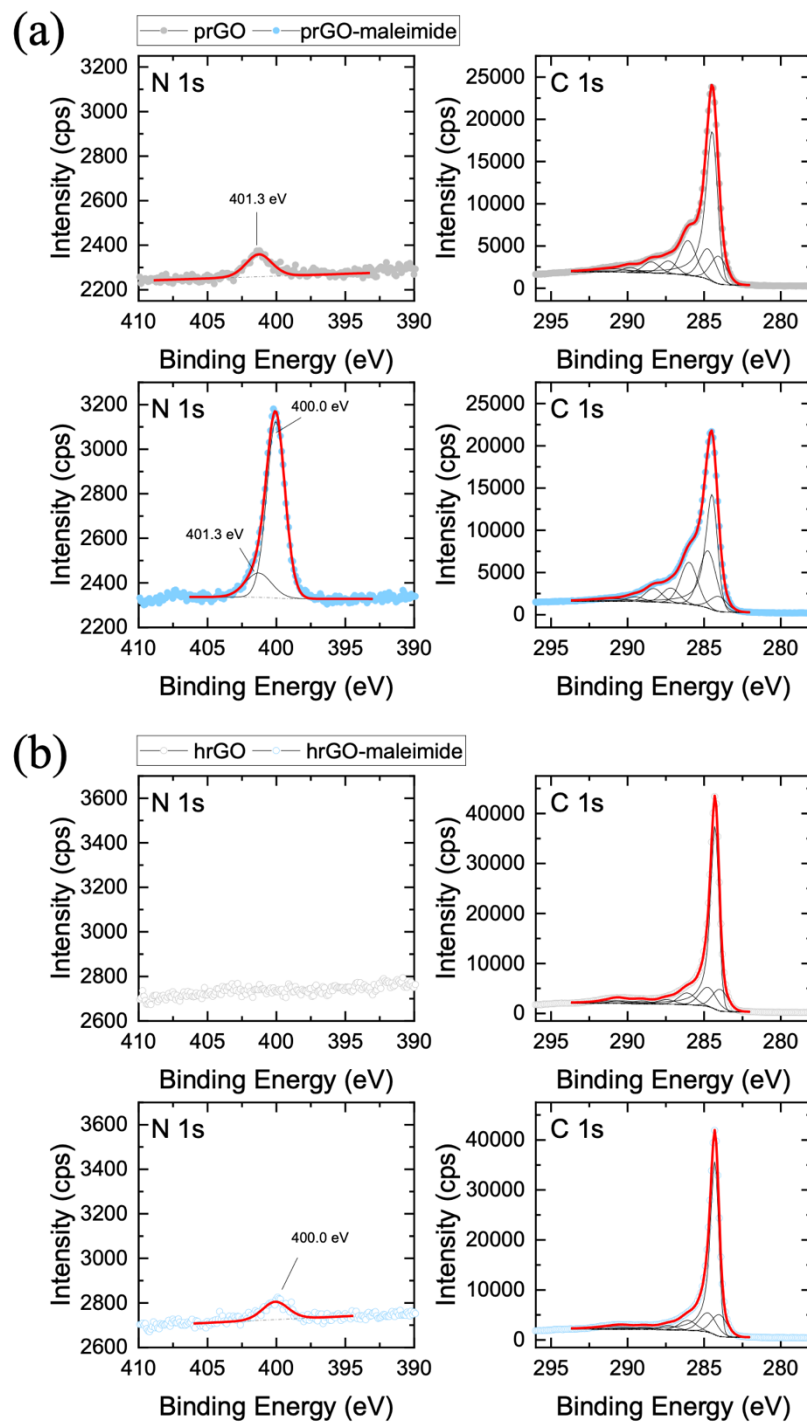**Figure 3** Raman analysis of (a) prGO and (b) hrGO functionalized with maleimide.

Figure 4 High-resolution XPS data collected on the (a) prGO and (b) hrGO samples, acquired over the binding energy regions typical for nitrogen (left) and carbon (right) main peaks, without (upper) and with (bottom) maleimide functionalization.

Table 1 Thermogravimetric and Raman analysis of prGO and hrGO before and after functionalization with maleimide derivative

Sample	Weight loss (%)	I_D/I_G	O (%)	C%	H%	N%
prGO	27.92	1.05	24.94	68.90	1.16	0.01
maleimide-prGO	30.72	0.88	25.03	69.91	1.53	1.03
hrGO	9.76	1.18	0.0	98.29	0.09	0.00
maleimide-hrGO	6.20	1.15	1.11	94.01	0.80	0.25

Table 2 X-ray photoelectron spectroscopy analysis of prGO and hrGO samples before and after functionalization with maleimide.

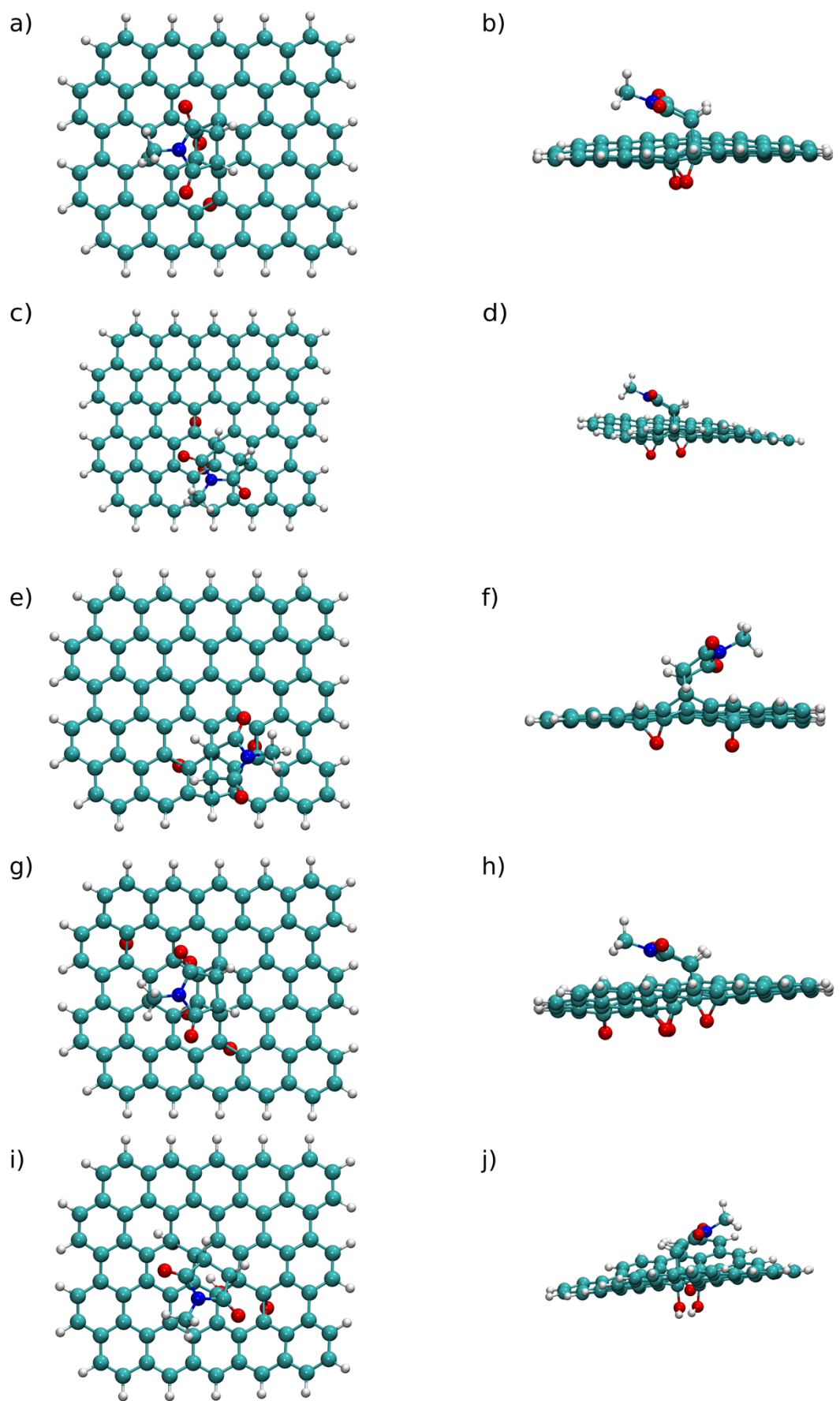| Component	Position (eV)	prGO	hrGO	prGO-maleimide	hrGO-maleimide
C=C	284.4±0.2	48.6%	61.7%	37.0%	61.0%
C vacancies	284.0±0.2	11.8%	12.8%	6.7%	13.8%
C-C	284.8±0.2	13.6%	12.8%	25.3%	13.6%
C-O; C-N	286.0±0.2	15.5%	7.8%	18.5%	7.0%
C=O	287.3±0.2	5.6%	3.0%	6.5%	2.9%
COOH	288.7±0.2	4.9%	1.9%	6.0%	1.7%

Figure 5 Top and side views of the optimized geometry of model (a,b) 7aP, (c,d) 7bP, (e,f) 8P, (g,h) 9P, and (i,j) 10P.

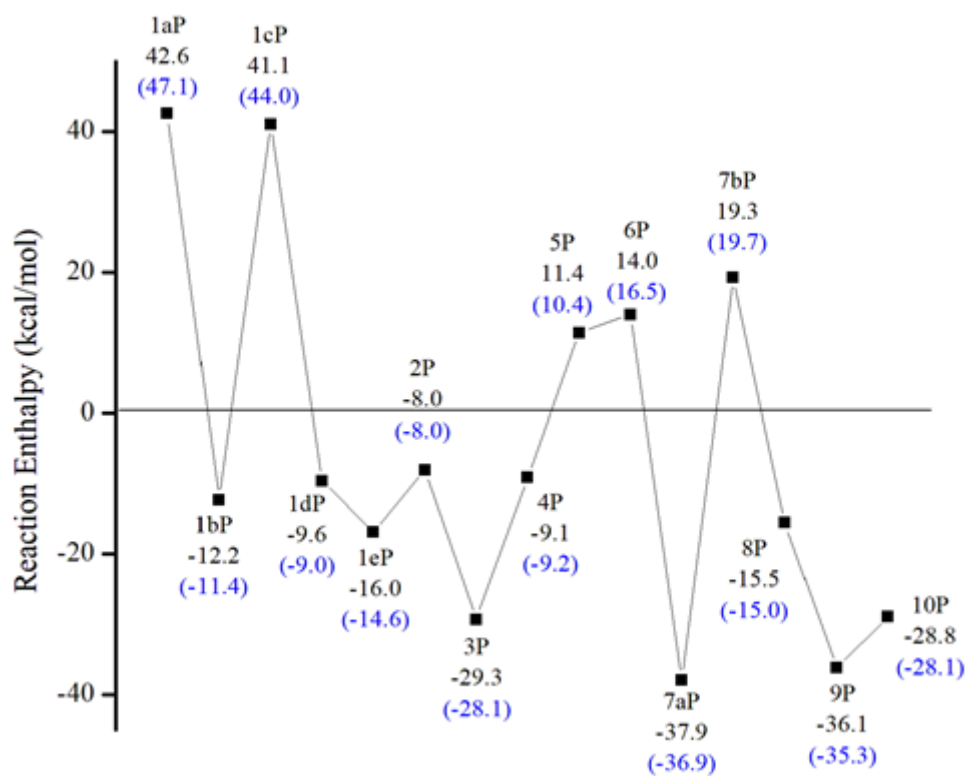**Figure 6** Reaction enthalpy (ΔH) of all maleimide-graphene adducts, evaluated in the gas-phase at $T = 25°C$. In parentheses (marked in blue), the same energy including the contribution of the solvent phase (i.e., chloroform) evaluated at $T = 50°C$.
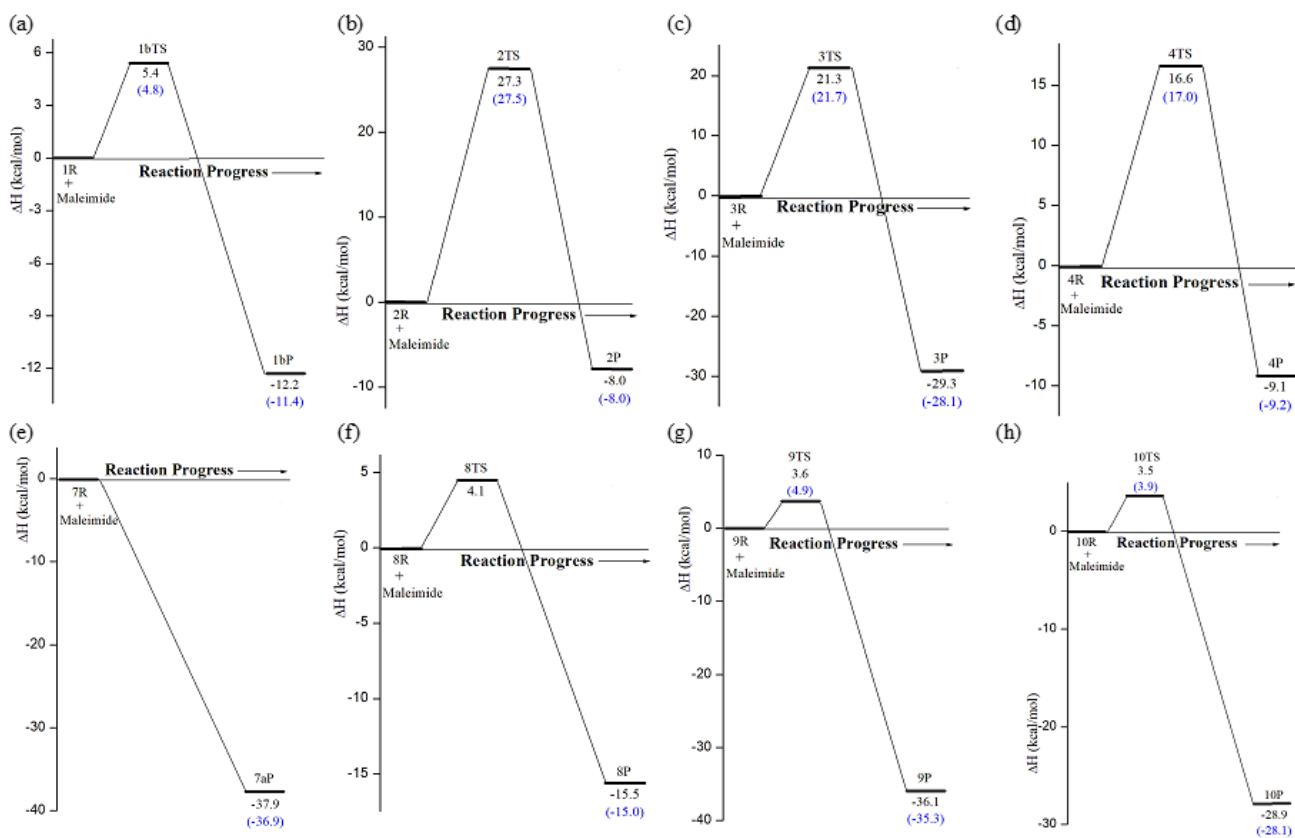
Figure 7 Enthalpy diagram of the DA cycloaddition reaction between maleimide and graphene considering only the models leading to exothermic reactions. The solvent-phase enthalpies are marked in blue.

Table 3 Rates of the DA cycloaddition reaction between maleimide and graphene.

Reaction	Gas-phase (298K)	Chloroform (323K)
1R → 1bP	3.11×10^{-3} s^{-1}	1.88×10^{-3} s^{-1}
2R → 2P	1.52×10^{-17} s^{-1}	3.91×10^{-16} s^{-1}
3R → 3P	6.23×10^{-14} s^{-1}	8.43×10^{-13} s^{-1}
4R → 4P	3.01×10^{-10} s^{-1}	1.82×10^{-9} s^{-1}
7R → 7P	2.01×10^{3} s^{-1}	4.3×10^{2} s^{-1}
8R → 8P	2.16×10^{-1} s^{-1}	1.29×10^{2} s^{-1}
9R → 9P	1.33×10^{-1} s^{-1}	3.28×10^{-2} s^{-1}
10R → 10P	1.84×10^{-1} s^{-1}	5.15×10^{-2} s^{-1}

Graphical TOC

Reduced Graphene Oxide + Maleimide → Maleimide-graphene

Diels-Alder cycloaddition